PCCP

Accepted Manuscript

ROYAL SOCIETY OF CHEMISTRY

www.rsc.org/pccp

Cite this: DOI: 10.1039/c0xx00000x

www.rsc.org/xxxxxx

ARTICLE TYPE

Hydrogen Photochromism in Nb_2O_5 powders

Lei Pan,[a] Yi Wang,[a] Xian Jie Wang,[b] HuiYing Qu,[c] JiuPeng Zhao,[c] Yao Li*[a] and Alexander Gavrilyuk*[d]

Received (in XXX, XXX) Xth XXXXXXXXX 20XX, Accepted Xth XXXXXXXXX 20XX
DOI: 10.1039/b000000x

In this paper, we report on the hydrogen photochromism of Nb_2O_5 powders with different structures. Four different powder phases were prepared by calcining $Nb_2O_5 \cdot nH_2O$ powders at various temperatures, and their morphology, structure, and electronic band structure were characterized by scanning electron microscopy, structural analyses, thermogravimetric analysis, differential scanning calorimetry, and optical spectroscopy. Nb_2O_5 powders with different structures and very different properties were formed after different high-temperature treatments of the polymorphous oxide. A pronounced photochromic effect was observed in the M and H phases of Nb_2O_5, whereas the other phases exhibited poor photochromic responses. Because the photochromism arises due to the detachment of hydrogen atoms under the action of light from hydrogen donor molecules previously adsorbed on the oxide surface, the electron band structure and the morphology have strong influences on the photochromic properties of the Nb_2O_5 powders. For these reasons, the pronounced photochromic effect was achieved in the H phase.

Introduction

Although photochromism in transition metal oxides (TMOs), to the best of our knowledge, was reported first for ZnO in the 19th century,[1] systematic and continuous investigations were only launched in the 1960s, when the photochromic TMOs started to attract attention for promising applications in many fields.[2] For example, potential applications include the production,[3] storage, and transport of hydrogen as a fuel, dopant, or catalyst for hydrogen energetics, biology, or medical applications, among many other possible applications in science and technology. WO_3 and MoO_3 are being studied especially intensively.[4-10] Some other TMOs such as V_2O_5[11] and TiO_2[12] were also reported to have photochromic properties. The results of the continuous research made it possible to forward several theoretical models for understanding the nature of the photochromism in TMOs.[1, 6, 13-16] The influences of various factors such as the preparation method,[17-20] crystal structure,[18, 19, 21] temperature,[16] morphology,[18] and electronic band structure[20] on the photochromic behavior were also investigated in detail.

It should be stressed that the photochromism of TMOs is very special in that it is due to detachment of hydrogen atoms from organic molecules previously adsorbed on the oxide surface under the action of light. These hydrogen atoms donate electrons to the oxides to form lower-valence cations, whereas the detached protons are localized in the vicinity of the oxygen anions.[16] The mechanism for the photoinjection of hydrogen that yields the photochromism was described in detail elsewhere[14,16] and determined as proton-coupled electron transfer. In fact, the photoinjection of hydrogen is a form of doping of the electron-proton plasma, which yields radical changes in the oxide parameters. In addition, the hydrogen photochromism may be a useful tool for investigations of hydrogen processes in the oxides.

In the hydrogen photoinjection process, the TMOs perform several functions related to the hydrogen behavior:

i. they serve as effective catalysts for hydrogen abstraction reactions under the action of light,
ii. having the friable structure, they are appropriate for accommodation of the large number of the detached protons,
iii. they provide transport of the injected hydrogen atoms

Niobium is a "relative" of vanadium in the periodic table of elements, both metals belonging to the group 5. Therefore it is reasonable to extend the research of photochromism in TMOs to Nb_2O_5. However, despite many ongoing investigations of the photochromism in V_2O_5, to the best of our knowledge, the photochromism in pure Nb_2O_5 was reported only once. Yao et al. prepared an amorphous Nb_2O_5 film by evaporation and discovered its photochromism.[22] Except for in this study, Nb_2O_5 has only been used as a dopant for other photochromic oxides.[23, 24] The photochromism in Nb_2O_5 is poorly investigated, since the effect appears to be relatively small as compared with those of other TMOs, and colored Nb_2O_5 films bleach rapidly upon exposure to oxygen-containing media,[22] which hampers experiments.

However, Nb_2O_5 is also a material of interest for both its electrochromism[25] and its photochromism, and its photochromic properties must therefore be understood and the influence of various factors upon the photochromic response should be investigated. Study of Nb_2O_5 is also necessary for a general understanding of the photochromism in TMOs.

The objective of the research was to prepare various Nb_2O_5 phases with different characteristics and to perform a comparative analysis of their hydrogen photochromism. For this reason, we selected powders instead of films. Preparation of various Nb_2O_5

phases requires high-temperature treatment, and by using the powders we avoid undesirable interactions between the films and the substrate, which could yield errors in the experiments.

Experimental

Preparation of the Nb_2O_5 powders

Except water, all reagents used in the experiments, namely, ammonium niobate (V) oxalate hydrate of 99.99% purity and ammonium hydroxide solution of 99.99% purity (28% NH_3 in H_2O), were commercial Sigma-Aldrich products. High-purity water with a resistivity of 18.2 MΩ·cm at 25°C was prepared by a water purification system.

The hydrous niobium oxide was precipitated from a 0.8 M ammonium niobate oxalate hydrate solution by addition of ammonium hydroxide solution (drop by drop) until the pH value became higher than 7. The precipitate was filtered, washed with pure water three times, and dried at room temperature. The prepared hydrous oxide was then calcined at various temperatures for 2 h to get different phase structure. The Nb_2O_5 samples calcined at 500°C, 600°C, 900°C, 1100°C, and 1300°C are labelled as P_{500}, P_{600}, P_{900}, P_{1100}, and P_{1300}, respectively.

Illumination of the samples

The Nb_2O_5 powders were pressed into tablets and placed in a cell with a quartz window. The cell was connected to a flask containing absolute ethanol and zeolite powder and pumped down to a 5 kPa pressure. At this pressure, the ethanol started to bubble. The zeolite powder was used to stabilize the bubbling process. After 10 minutes of ventilation with ethanol vapor, the sample was illuminated by the full output of a 250 W high-pressure mercury lamp. Then, the illuminated samples were taken out of the cell and investigated using the diffuse reflection method.

Characterization of the samples

The combined thermogravimetric differential scanning calorimetry (TGA-DSC) analysis was performed using an STA8000 device (Perkin Elmer Inc.) at a 10°C /min scan rate over the 25–1330°C range with a 25 mL/min flow of nitrogen of 99.99% purity. The crystalline structure of the powder was analyzed by D/Max-rB X-ray diffractometer (Cu K_α radiation) at a 5°/min scan rate. The diffuse reflection spectra in the UV range used for the band gap calculations were measured by a Lambda 950 spectrophotometer with an integrating sphere. Scanning electron microscope (SEM) images were obtained with the help of a Hitachi SU 8010 microscope operated at a 15 kV voltage.

Results and discussion

Phase transformation of the Nb_2O_5 powders

Nb_2O_5 has at least 12 different polymorphic forms[25], in which the T[26], TT[27], B[28], M[29] and H[30] phases are most commonly observed. Among these phases, the H phase is the most thermodynamically stable at atmospheric pressure.[31]

The thermogravimetric analysis-differential scanning calorimetry (TG-DSC) curves registered simultaneously for the hydrous niobium pentoxide powders are presented in Fig. 1. Most of the H_2O and NH_3 molecules adsorbed on the oxide surface[32] were evolved from the surface at T < 500°C, which yielded a 23.0% mass loss. The DSC curve shows three main peaks at T > 500°C. Only a 1.3% mass loss was registered in the range between 500 and 1300°C. The first exothermic peak at 584°C is attributed to the crystallization of the quasi amorphous powder to the TT crystalline phase (PDF#28-0317, P, pseudo-hexagonal)[27], which is proved by the X-ray diffraction (XRD) analysis (see Figs 2a and 2b). The second peak (endothermic) at 1075°C is due to the phase transformation from the TT phase to the M phase (PDF#32-0711, I4/mmm, tetragonal)[29], which is also confirmed by the XRD analysis (see Fig 2d). The third peak (exothermic) at 1243°C is attributed to the formation of the H phase (PDF#37-1468, P2/3, monoclinic)[30] from the M phase, which is again confirmed by the XRD results. The XRD pattern of the P_{900} phase shows a mixture of the TT and M phases, indicating that the powders are undergoing the phase transformation. This is confirmed by the heat flow enhancement in the high temperature range, namely from ≈800°C to ≈1075°C (see the DSC curve). Since P_{900} is a mixture of the two other phases we did not investigate it further; our objectives were to study the photochromic properties of "pure" phases.

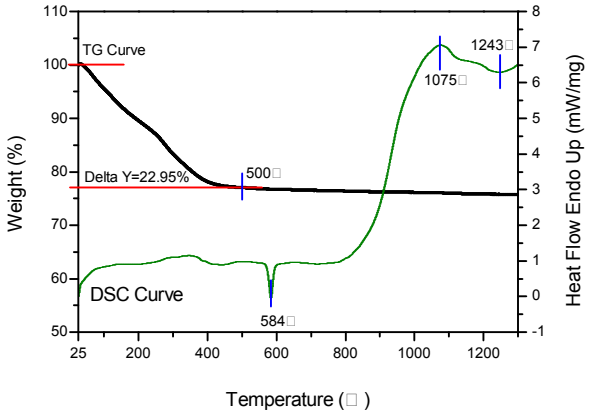

Fig. 1 Thermogravimetric analysis-differential scanning calorimetry (TG-DSC) curves of the hydrous Nb_2O_5 powders.

The SEM images in Fig. 3 show the morphologies of the powders. The grain size of the Nb_2O_5 powders obviously continuously increases with increasing calcination temperature. The relation between the grain size and the photochromic properties of the Nb_2O_5 powders will be discussed below.

Band gaps in the Nb_2O_5 powders

The photochromism in the TMO is triggered by the photogenerated electron-hole pairs, as was found for the WO_3 and the V_2O_5 films.[14, 16, 22] We hypothesize that the main reason for the poor photochromic sensitivity and quick bleaching in Nb_2O_5 is that Nb_2O_5 has an electron work function much smaller than those for WO_3, MoO_3, and V_2O_5. In particular, its conduction band potential lies close to that for TiO_2.[33] Therefore, as Fig. 4 shows, despite the band gap width values are close in Nb_2O_5 and in photochromic highly disordered WO_3 films (see our results below and reference[34, 35]) the electron injected into the Nb_2O_5 conduction band has a higher predisposition than in other oxide,

e.g., to participate in backward and secondary reactions, which in turn reduces the photochromic sensitivity.

Furthermore, the oxide band gap width is an important parameter that greatly influences the photochromic process. The band gap value of Nb_2O_5 varies between 2.35 eV and 4.2 eV in different reports,[25, 36-39] depending on different preparation methods and morphologies. Therefore, it is important to determine the band gap values of different samples to investigate their photochromic properties.

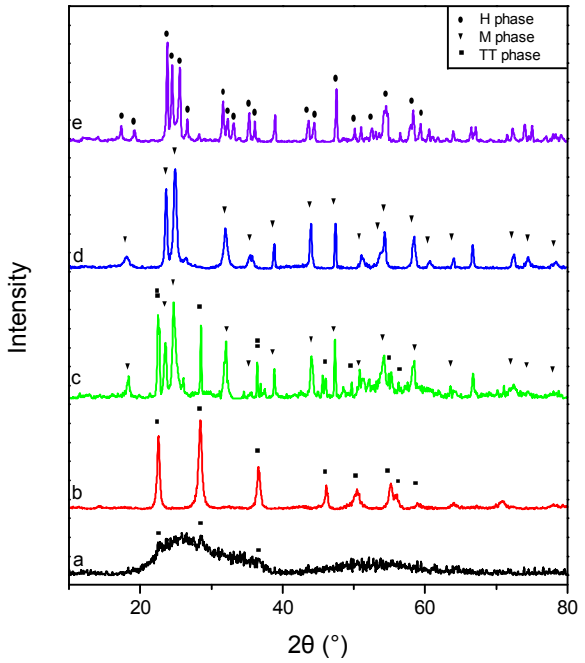

Fig. 2 X-ray diffraction (XRD) patterns for the Nb_2O_5 powders: (a) P_{500}, (b) P_{600}, (c) P_{900}, (d) P_{1100} and (e) P_{1300}.

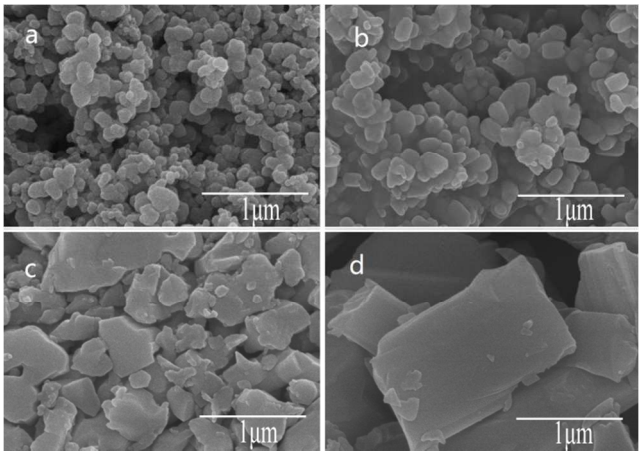

Fig. 3 Scanning electron microscopy (SEM) images for the Nb_2O_5 powders: (a) P_{500}, (b) P_{600}, (c) P_{1100} and (d) P_{1300}.

The diffuse reflection spectra of different Nb_2O_5 powders were measured and converted into the Kubelka-Munk function ($F(R)$) by the equation[37]

$$F(R) = (1-R)^2/2R.$$

The plots of $(F(R)hv)^2$ versus hv for different samples are given in Fig. 5. The band gap width (E_g) values were obtained by extrapolating the linear part of the plot to $(F(R)hv)^2 = 0$.[37] Fig. 5 shows that the E_g values for P_{500}, P_{600}, P_{1100}, and P_{1300} are 3.49, 3.55, 3.34, and 3.23 eV, respectively.

Despite the low accuracy of this method, there is a noticeable difference in the band gap values between the two phases calcined at high temperatures and the two phases calcined at low temperatures. This is also confirmed by the experiment described in the next section.

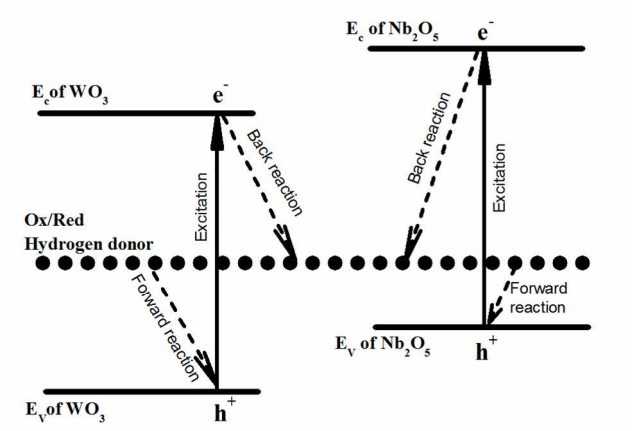

Fig.4. Schematic of the electronic band structure for WO_3 disordered films and Nb_2O_5 powders.

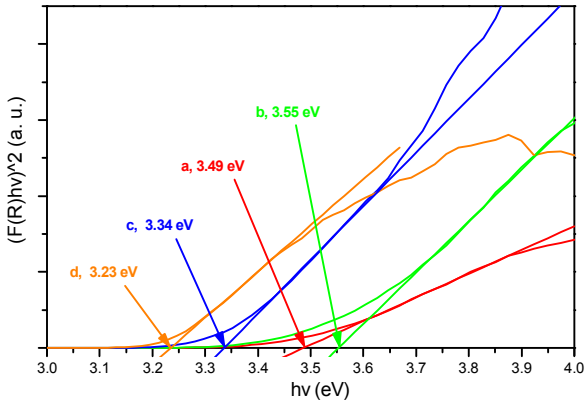

Fig. 5 Plots of $(F(R)hv)^2$ versus energy (hv) for determination of the band gap values of the Nb_2O_5 powders: (a) P_{500}, (b) P_{600}, (c) P_{1100} and (d) P_{1300}.

Fig. 6 Visual appearance of the P_{1100} powders (left image) illuminated through the mask (right image).

Photochromism in the Nb_2O_5 powders

The photochromic responses of P_{500}, P_{600}, P_{1100}, and P_{1300} were examined. As-prepared hydrous Nb_2O_5 powders are white and preserve their color after calcination at temperatures up to 1200°C, whereas the samples calcined at 1300°C become slightly yellowish. The illumination of P_{1300} and P_{1100} in ethanol vapor caused the samples to acquire a deep blue color. The colored P_{1100} is shown in Fig. 6. The illumination of P_{500} in ethanol vapor caused a similar but much attenuated effect, whereas P_{600} did not exhibit photochromism. The photochromic response was not observed under illumination in air, nitrogen, water vapor, or a mixture of air and ethanol vapor for any investigated sample.

The diffuse reflection spectra for P_{1100} before and after illumination are presented in Fig. 7a, which shows that the reflection decreases gradually in the whole visible–near infrared range with exposure, although the reflection in the red part of the spectrum is definitely much smaller than that in the blue part. For this reason, the powder acquires a blue color that continuously becomes deeper with illumination time.

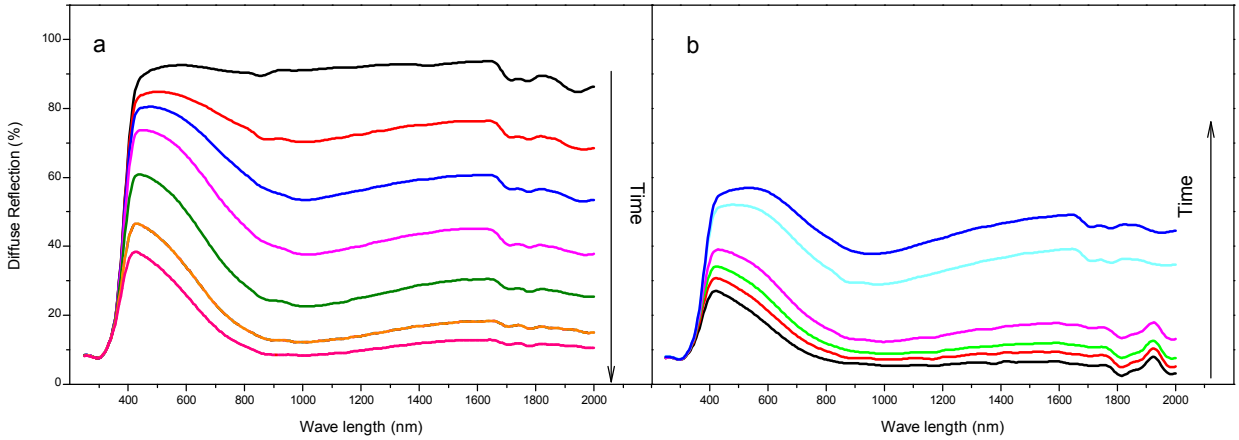

Fig. 7. Diffuse reflection spectra of P_{1100} powders measured along (a) the coloration process and (b) the bleaching process. (a) Illumination times are 0, 2, 5, 10, 20, 60 and 300 min, correspondingly (from top to bottom) and (b) bleaching times are 0, 12, 50, 180, 870, and 1230 min, correspondingly (from bottom to top).

The coloration of the TMOs upon insertion of hydrogen atoms is attributed to the appearance of the lower-valence cations,[1,5] and, in turn, to the optical transitions between neighboring non-isovalent cations. For Nb_2O_5, these are the transitions between Nb^{4+} and Nb^{5+} cations:

$$Nb^{4+}(A) + Nb^{5+}(B) \overset{h\nu}{\leftrightarrow} Nb^{5+}(A) + Nb^{4+}(B)$$

Bleaching of the colored Nb_2O_5 powders can be observed in the presence of oxygen, as was reported for amorphous Nb_2O_5 films,[22] but in P_{1100} and P_{1300} this process was much slower. The diffuse reflection spectra for the colored P_{1100} measured at various times in the bleaching process are shown in Fig. 7b. The color barely changed when the sample was held in air for several hours. After one week of storage in air, the colored P_{1100} was still light blue. Full bleaching was achieved after approximately two weeks of storage in air. At 80°C, the bleaching can be essentially accelerated, and the samples return to their initial colors after ≈24 h. The bleaching in air occurs through oxidation of the formed niobium hydrogen bronze $H_xNb_2O_5$:

$$H_xNb_2O_5 + x/2\ O_2 \rightarrow Nb_2O_5 + x/2\ H_2O.$$

The coloration-bleaching process is reversible, and we did not notice any decay of the photochromic sensitivities of P_{1100} and P_{1300} over at least five coloration-bleaching cycles. The diffuse reflection spectra for the coloration and bleaching processes in P_{1300} were also measured, but are not presented here since they are very similar to those of P_{1100}.

To illustrate the kinetics of the coloration and bleaching of the Nb_2O_5 powders, the areas between each reflection spectrum in coloration process and the reflection spectrum of the as-prepared P_{1100} or P_{1300} were integrated, and the obtained values Δ were plotted against the illumination time *t* in Fig 8a; the areas between each reflection spectrum in bleaching process and the reflection spectrum of the colored P_{1100} or P_{1300} before bleaching were integrated, and the obtained values Δ were plotted against the bleaching time *t* in Fig 8 b. Fig. 8a shows that the maximum reaction rate occurs at the very beginning of the coloration process.

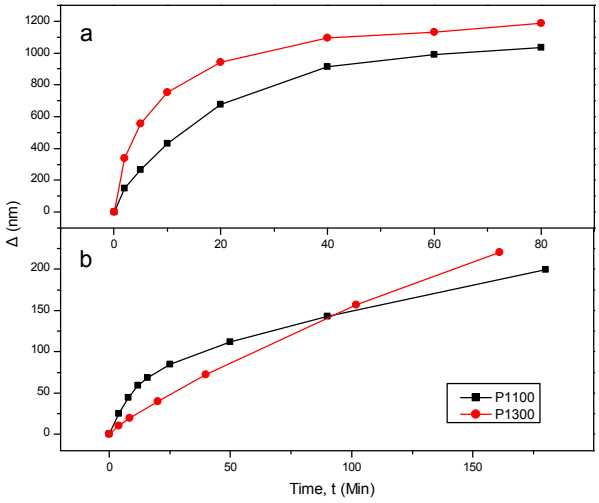

Fig. 8 The changes in the integrated diffuse reflection Δ, of the Nb_2O_5 powders along (a) coloration process and (b) bleaching process.

This kinetic behaviour is very similar to that found for the other TMOs and is typical for photochemical reactions driven by holes. For such reactions, the reaction rate decreases with increasing Fermi level.[40] The higher position of the conduction band potential in Nb_2O_5 leads to a higher Fermi level. Thus, the equilibrium state can be achieved for the hydrogenation reaction under the action of light:

$$Nb_2O_5 + RH + h\nu \leftrightarrow H_xNb_2O_5 + RH_{1-x}$$

where R denotes the radicals formed when hydrogen atoms are detached from the hydrogen donor molecules and x is the non-stoichiometric parameter. When the equilibrium between the forward and backward reactions is achieved, the hydrogenation process is stopped. The higher the position of the Fermi level, the faster the equilibrium is achieved.

The fact that no photochromism is observed under illumination in a mixture of air and ethanol vapor indicates that the oxidation of the detached hydrogen atoms is faster than their photoinduced splitting from ethanol molecules. This is a very important finding, since the other photochromic TMOs exhibit photochromism in the presence of air if hydrogen donor molecules are adsorbed on their surfaces. We attribute this result to the high conduction band potential in Nb_2O_5 as compared with those of other TMOs. The bleaching rate may be retarded by diffusion of the injected hydrogen atoms inside of the grains, which can be accelerated by increasing the temperature or decreasing the particle size.

The photochromism in Nb_2O_5 exhibits some very interesting paradoxes. Generally, amorphous TMOs have higher photochromic sensitivities because of their higher specific surface areas.[19, 21] The specific surface area is a very important factor influencing the photochromic sensitivity, since the higher the surface area is, the more reactive centers exist on the surface for the photoinjection of hydrogen into the oxide. However, the amorphous Nb_2O_5 sample (P_{500}) showed a lower coloration efficiency than the M phase (P_{1100}) or the H phase (P_{1300}). After 2 h of illumination, the maximum coloration was achieved in P_{500}, which was similar to the coloration of P_{1100} after 5 min of illumination. P_{500} exhibits noticeable bleaching in the first few seconds after the sample is exposed to air. Full bleaching of the colored P_{500} occurred in several minutes. For this reason, the reflection was not measured for colored P_{500} in this research.

There are several reasons for such behavior of P_{500}. First, it has a higher E_g than P_{1100} or P_{1300}. The spectrum of a high-pressure mercury lamp contains a series of bands in the UV range, and the band at 3.40 eV (λ=365 nm) is the most intense.[41] However, this irradiation band cannot efficiently generate electron-hole pairs in P_{500}, since the energy of the photons is less than the band gap. When we replaced the quartz window of the cell with toughened glass to exclude irradiation by photons with energies E_g= 3.40 eV, P_{500} showed no photochromic response. This experiment also proved that the accuracy of the test for the band gap value is sufficient to support our conclusions. Second, the larger bandwidth indicates a higher Fermi level of the injected electrons, which in turn leads to their higher reactivity in the backward surface reactions, which reduces the photochromic sensitivity. There is a clear correlation between the band gap value and the photochromic properties: the phases with higher E_g (P_{500} and P_{600}) have either no or poor photochromic responses, whereas the phases with the lower E_g possess good photochromic properties.

On the other hand, the morphology of the P_{1100} and P_{1300} phase can also retard the rise in the Fermi level under illumination. Because of the structural disorder in the P_{500} and P_{600} phases, there are a large number of surface defects in these phases (see Fig. 3a) that may serve as traps for the injected particles and hamper their diffusion into the oxide bulk. The activity of the injected electrons in the backward reactions is determined by the Fermi level on the oxide surface. Diffusion of the electron-proton plasma can reduce the Fermi level on the oxide surface and retard the rise in the Fermi level due to hydrogenation. Thus, the diffusion of the plasma can be helpful in the coloration process.

The fast bleaching of colored P_{500} may be also attributed to the small grain size. The grain size of P_{500} in Fig. 3a is much smaller than the grain sizes of P_{1100} or P_{1300} (Fig. 3b). It would take much more time for the inserted protons and electrons to diffuse from the grain bulk of these large particles to the oxide surface. For this reason, these different phases exhibit greatly different bleaching processes.

In summary, the main parameter influencing the photochromic response in the polymorphous Nb_2O_5 phases is the electron band structure, whereas the electron-proton plasma diffusion, grain size, and morphology have smaller influences on the hydrogenation and dehydrogenation processes.

Conclusions

For the first time, it was shown that the different Nb_2O_5 phases exhibit very different photochromic properties that depend upon the oxide band gap value. We achieved the highest ever reported photochromic response for the P_{1100} and P_{1300} Nb_2O_5 phases. We investigated the kinetics of the photocoloration and bleaching in these phases and demonstrated that these processes are reversible.

The most important achievement in this research is the isolation of the photochromic Nb_2O_5 phase among the different Nb_2O_5 phases. For this phase, the hydrogen photochromism will be investigated more deeply using other methods in future research.

Acknowledgements

We thank National Natural Science Foundation of China (No. 51010005, 91216123, 51174063), Natural Science Funds for Distinguished Young Scholar of Heilongjiang province, the Natural Science Foundation of Heilongjiang Province (E201436) and the project of International Cooperation supported by Ministry of Science and Technology of China (2013DFR10630).

Notes and references

[a] *Center for Composite Materials and Structures, Harbin Institute of Technology, Harbin 150080, China*
[b] *Department of Physics, Harbin Institute of Technology, Harbin 150080, China*
[c] *School of Chemical Engineering and Technology, Harbin Institute of Technology, Harbin 150001, China,*
[d] *A.F. Ioffe Physical Technical Institute of Russian Academy of Sciences, 194021 Polytekhnicheskaya Street 26, Sankt-Petersburg, Russia*
**To whom the correspondence should be addressed:* Yaoli@hit.edu.cn, Gavrilyuk@mail.ioffe.ru

1. T. He and J. N. Yao, *Res Chem Intermediat*, 2004, **30**, 459-488.
2. J. N. Yao, K. Hashimoto and A. Fujishima, *Nature*, 1992, **355**, 624-626.
3. Z. G. Yi, H. Iwai and J. H. Ye, *Appl Phys Lett*, 2010, **96**.
4. K. Bange, *Sol Energ Mat Sol C*, 1999, **58**, 1-131.
5. S. T. Wang, X. J. Feng, J. N. Yao and L. Jiang, *Angew Chem Int Edit*, 2006, **45**, 1264-1267.
6. T. He and J. N. Yao, *J Photoch Photobio C*, 2003, **4**, 125-143.
7. A. I. Gavrilyuk and M. M. Afanasiev, *Sol Energ Mat Sol C*, 2009, **93**, 280-288.
8. U. Tritthart, W. Gey and A. Gavrilyuk, *Ionics*, 1998, **4**, 299-308.
9. A. I. Gavrilyuk, *Sol Energ Mat Sol C*, 2009, **93**, 1885-1895.
10. J. Scarminio, *Sol Energ Mat Sol C*, 2003, **79**, 357-368.
11. A. Gavrilyuk, U. Tritthart and W. Gey, *Phys Chem Chem Phys*, 2011, **13**, 9490-9497.
12. J. G. Highfield and M. Gratzel, *J Phys Chem-Us*, 1988, **92**, 464-467.
13. A. Gavrilyuk, *Optical Organic and Semiconductor Inorganic Materials*, 1997, **2968**, 195-200.
14. A. I. Gavrilyuk, U. Tritthart and W. Gey, *Phil Mag Lett*, 2006, **86**, 205-214.
15. K. Kim, C. Seo and H. Cheong, *J Korean Phys Soc*, 2006, **48**, 1657-1660.
16. A. Gavrilyuk, U. Tritthart and W. Gey, *Philos Mag*, 2007, **87**, 4519-4553.
17. S. Nowak, J. Zmija, T. Kaczor and T. Lukasiewicz, *Solid State Crystals: Growth and Characterization*, 1997, **3178**, 193-195.
18. L. Miao, S. Tanemura, T. Jiang, M. Tanemura, K. Yoshida, R. Huang and G. Xu, *2008 2nd Ieee International Nanoelectronics Conference, Vols 1-3*, 2008, 1093-1098.
19. N. N. Dinh, V. T. Bich, N. H. Hoang and L. Q. Minh, *Phys Status Solidi A*, 1988, **108**, K157-K161.
20. T. J. DeJournett and J. B. Spicer, *Sol Energ Mat Sol C*, 2014, **120**, 102-108.
21. E. Kikuchi, K. Iida, A. Fujishima and K. Itoh, *J Electroanal Chem*, 1993, **351**, 105-114.
22. J. N. Yao, B. H. Loo, K. Hashimoto and A. Fujishima, *Ber Bunsen Phys Chem*, 1992, **96**, 699-701.
23. C. O. Avellaneda and L. O. S. Bulhoes, *Solid State Ionics*, 2003, **165**, 117-121.
24. N. A. Papunashvili, V. D. Ryabtseva, N. A. Sikharulidze and A. L. Shengeliya, *Glass Phys Chem+*, 1999, **25**, 449-453.
25. M. A. Aegerter, *Sol Energ Mat Sol C*, 2001, **68**, 401-422.
26. K. Kato and S. Tamura, *Acta Crystallogr.*, 1975, **31**, 673-677.
27. L. K. frevel and H. W. Rinn, *Analytical Chemistry*, 1955, **27**, 1329-1330.
28. F. Laves, W. Petter and H. Wulf, *Die Naturwissenschaften*, 1964, **51**, 633-634.
29. M. Ritschel and H. Oppermann, *Kristall und Technik*, 1978, **13**, 1035–1043.
30. B. M. Gatehouse and A. D. Wadsley, *Acta Crystallographica*, 1964, **17**, 1545-1554.
31. C. Valencia-Balvín, S. Pérez-Walton, G. M. Dalpian and J. M. Osorio-Guillén, *Computational Materials Science*, 2014, **81**, 133-140.
32. W. Qi, J. Heng, G. Hong and S. Tingting, *Analytical instrumentation*, 2011, 28-32.
33. S. Furukawa, T. Shishido, K. Teramura and T. Tanaka, *Acs Catal*, 2012, **2**, 175-179.
34. C. G. Granqvist, *Handbook of inorganic electrochromic materials*, Elsevier, 1995. *p.141*.
35. G. A. Niklasson and C. G. Granqvist, *J Mater Chem*, 2007, **17**, 127-156.
36. R. Brayner and F. Bozon-Verduraz, *Phys Chem Chem Phys*, 2003, **5**, 1457-1466.
37. P. S. Patil, A. R. Patil, S. H. Mujawar and S. B. Sadale, *J Mater Sci-Mater El*, 2005, **16**, 35-41.
38. K. Yoshimura, T. Miki, S. Iwama and S. Tanemura, *Thin Solid Films*, 1996, **281-282**, 235-238.
39. H. Mizoguchi, M. Orita, M. Hirano, S. Fujitsu, T. Takeuchi and H. Hosono, *Appl Phys Lett*, 2002, **80**, 4732-4734.
40. A. I. Gavrilyuk, *Electrochim Acta*, 1999, **44**, 3027-3037.
41. A. I. Gavrilyuk, *Sol Energ Mat Sol C*, 2010, **94**, 515-523.